Macromolecules
ARTICLE

Macromolecules **2010**, *43*, 7807–7812 **7807**
DOI: 10.1021/ma101529b

Solvent-Driven Evolution of Block Copolymer Morphology under 3D Confinement

Le Li,[†] Kazuyuki Matsunaga,[‡] Jintao Zhu,[†] Takeshi Higuchi,[§] Hiroshi Yabu,[⊥] Masatsugu Shimomura,[§] Hiroshi Jinnai,[‡,§] Ryan C. Hayward,*[,†] and Thomas P. Russell*[,†,§]

[†]*Department of Polymer Science and Engineering, University of Massachusetts, Amherst, Massachusetts 01003,* [‡]*Department of Macromolecular Science and Engineering, Graduate School of Science and Engineering, Kyoto Institute of Technology, Kyoto 606-8585, Japan,* [§]*World Premier International Research Center, Advanced Institute for Materials Research (WPI-AIMR), Tohoku University, Sendai 980-8577, Japan,* [⊥]*Institute of Multidisciplinary Research for Advanced Materials (IMRAM), Tohoku University, Sendai 980-8577, Japan, and Precursory Research for Embryonic Science and Technology (PRESTO), Japan Science and Technology Agency (JST), Kawaguchi, Saitama 332-0012, Japan*

Received July 8, 2010; Revised Manuscript Received August 4, 2010

ABSTRACT: Nanoparticles with concentric layered structures were generated from a lamellae-forming poly(styrene-*b*-isoprene) diblock copolymer using controlled precipitation from a tetrahydrofuran/water mixture. Chloroform, a good solvent for both blocks, was used to swell and anneal the nanoparticles suspended in aqueous media. The three-dimensional morphologies of particles were reconstructed by transmission electron microtomography throughout the process of solvent annealing. A transition from concentric lamellae to PI cylinders in a PS matrix occurred upon annealing, presumably due to a slight selectivity of chloroform for PS. These cylindrical microdomains were further divided into PS-core−PI-shell spherical structures in a PS matrix upon extended annealing, a structure that is unique among reported microphase separated morphologies of diblock copolymers.

Introduction

Block copolymers (BCPs) undergo bulk microphase separation into spherical, cylindrical, gyroid, and lamellar microdomains, depending on the volume fraction of the components and degree of incompatibility between blocks.[1] Confinement can be used to break the symmetry so as to generate novel morphologies that cannot be obtained in the bulk. One-dimensional (1D) confinement, i.e., thin films confined between two planar surfaces,[2−6] is the most explored system to date where the boundary conditions are dictated by the film thickness and interfacial interactions. 2D confined systems have also been theoretically[7−11] and experimentally[12−16] investigated. Helical morphologies were observed under cylindrical confinement[13,15] and predicted theoretically.[8−11] 3D confinement was initially investigated by an aerosol approach,[17] where small droplets were formed by spraying a solution and the solvent evaporated to yield spheres in which the BCP microphase separated. Numerous computational studies have appeared[18−21] that have been augmented by the development of several approaches to realize 3D confinement, including emulsion methods,[22−25] reprecipitation[26,27] and colloidal crystal templating.[28,29] In a confined geometry with imposed curvature, BCP with bulk lamellar structures tends to conform to the geometry, forming onion-like morphologies,[23] concentric cylindrical morphologies, unidirectionally stacked layers,[25,26] and lamellae oriented parallel to or normal to the walls confining the BCP.[28] Confinement also produces multilength scaled morphologies defined macroscopically by the geometry of the confinement volume and nanoscopically by the dimensions of the individual microdomains.

*To whom correspondence should be addressed. (R.C.H.) Telephone: 413-577-1317. Fax: 413-545-0082. E-mail: rhayward@mail.pse.umass.edu. (T.P.R.) Telephone: 413-577-1511. Fax: 413-577-1510. E-mail: russell@mail.pse.umass.edu.

A fundamental understanding of the relationship between the confinement conditions and the resulting structures will enable the use of these unconventional morphologies as templates or scaffolds for the fabrication of nanostructured materials. Efforts have been made to tune BCP morphologies by use of external fields such as surface patterning,[30] template guidance,[5,6] and electric fields,[6,31] among others. Solvent annealing[32−35] is one of the most common approaches to obtain well-ordered structures in thin films. Solvent gradients produced during evaporation[34] can effectively be used to control the orientation of the microdomains, while solvent quality can be used to control lateral ordering and the nature of the morphology produced. Solvent quality also affects the degree of incompatibility between blocks, as expressed by the effective Flory−Huggins interaction parameter χ_{eff}, and hence the phase behavior.[33,35] In 2D and 3D confinement, the degree of confinement[14,15,27,28] and interfacial interactions[23,25,29] have been used to influence morphologies produced but little efforts have been made to control the morphology of BCP nanoparticles by solvent annealing. Using an organic solvent to anneal BCP nanoparticles is challenging due to the potential for coalescence of the nanoparticles that accompanies solvation. Arsenault, Rider, et al.[28,29] used a combination of toluene vapor and thermal annealing of BCPs in colloidal crystal templates to achieve to promote the self-assembly of BCP, but removal of the solvent, along with the significant volume contraction, within a hard boundary will lead to nonequilibrium structures.

Here we introduce a new method for solvent-annealing of BCPs under soft 3D spherical nanoconfinement, i.e., where the volume defining confinement will be dictated by the extent of solvent swelling, and present results on the morphological evolution of a nearly symmetric poly(styrene-*b*-isoprene) (PS-*b*-PI) diblock copolymer upon annealing with a good solvent. Transmission electron microtomography (TEMT)[36,37] was used to

Published on Web 08/19/2010

Scheme 1. Nanoparticle Preparation (a) and Solvent Annealing Setup (b)

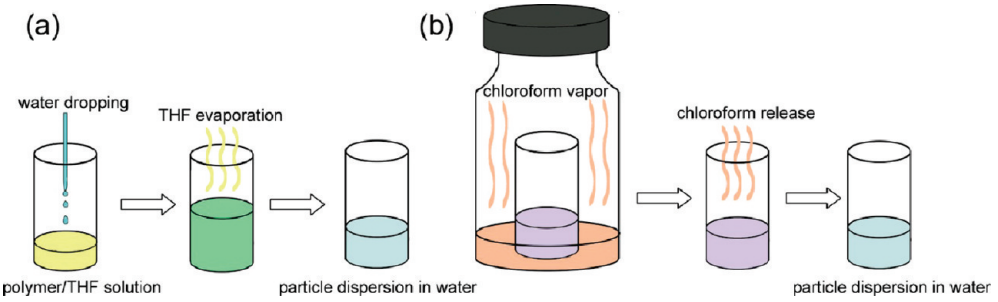

elucidate the 3-D nanostructures resulting from the spherical confinement. With increasing time of annealing, an ordering transition was found from onion-like structures, containing alternating PS and PI layers, to curved PI cylinders in a PS matrix, and ultimately to a novel morphology of PI-shell/PS-core spheres dispersed in a PS matrix. A mechanism of the ordering transition under 3D confinement is proposed and the origin of the final morphology of core/shell spheres is discussed. The results presented in this study demonstrate a useful new methodology for tuning structure in 3D nanoconfined BCPs and underscore the importance of solvent quality in generating unique morphologies in such systems.

Experimental Section

A nearly symmetric block copolymer polystyrene-*block*-polyisoprene (PS-*b*-PI) (Polymer Source, Inc., Canada) was used, with a PS number-average molecular weight of 25800 g/mol and PI of 20100 g/mol, and a polydispersity index of 1.08. The BCP nanoparticles were formed as aqueous suspensions by controlled precipitation from a good/poor solvent mixture of tetrahydrofuran (THF)/water.[26] In a typical experiment, 4 mL of deionized water was added dropwise into 1 mL of PS-*b*-PI/THF solution with a concentration of 0.1 mg/mL under stirring. THF was then allowed to slowly evaporate for more than 1 week at room temperature. To carry out solvent annealing, 500 μL of the BCP nanoparticle aqueous suspension (with a particle content of about 0.05 mg/mL) in a small vial was placed inside a large vial containing 1 mL of chloroform. The outer vial was sealed for a certain time recorded as the annealing time. Afterward, the inner vial was taken out to ambient atmosphere to release the absorbed chloroform. The sample preparation and annealing procedures are shown in Scheme 1.

To probe the internal structures, nanoparticles were collected onto copper grids supported with carbon film, dried, and stained by vapor of 4 wt % OsO_4 aqueous solution for 1 h. The double bonds in PI were cross-linked by OsO_4, leading to a darker appearance in transmission electron microscopy (TEM) images. To obtain cross-sectional structures, prestained nanoparticles were embedded into an epoxy resin, and cured at 60 °C for 24 h. Ultrathin sections were obtained by using a Leica Ultracut microtome equipped with a diamond knife. Bright field TEM measurements were conducted with a JEOL 200CX TEM operated at an accelerating voltage of 200 kV.

Prior to TEMT observation, a thin layer of carbon was evaporated onto the standard TEM sample to enhance heat transfer and reduce sample damage during long time exposure to the electron beam. Subsequently, gold particles (diameter ~10 nm, GCN005, BBInternational Co., Ltd., U.K.) were spread on the grids as markers. The experiments were carried out on a JEM-2200FS (JEOL Co., Ltd., Japan) operated at 200 kV and equipped with a slow-scan CCD camera (Gatan USC1000, Gatan Inc., USA). Only the transmitted and elastically scattered electrons (electron energy loss of 0 ± 15 eV) were selected by the energy filter (Omega filter, JEOL Co., Ltd., Japan). The tilt-angle ranges from $-65°$ to $+65°$ with 1° increment. All alignment and reconstruction procedures were carried out using software previously developed.[38]

The sizes of the nanoparticles during solvent annealing were measured by dynamic light scattering (DLS), as a means of tracking the degree of swelling with annealing time. The measurements were performed with an ALV unit equipped with an ALV/SP-125 precision goniometer (ALV-GmbH), Innova 70 argon laser (λ = 514.5 nm; maximum power, 3 W; Coherent Inc.) operated at 30 mW, and a photomultiplier detector (Thorn EMI electron tubes). Signals at 90° scattering angle were analyzed by an ALV 5000 Multiple Tau digital correlator board and associated software. The samples were transferred to the testing tubes directly from the annealing setup, sealed immediately, and tested without any treatment or dilution.

Small angle X-ray scattering (SAXS) patterns of bulk PS-*b*-PI swollen with chloroform were obtained from an Osmic MaxFlux X-ray source with a wavelength of 1.54 Å (Molecular Metrology, Inc.) and a camera consisting of a three-pinhole collimation system. The detector was a two-dimensional, multiwire proportional detector (Molecular Metrology, Inc.) and the sample-to-detector distance was 150 cm (calibrated using silver behenate).

Results and Discussion

1. Onion-Like BCP Nanoparticles. The initial formation of block copolymer nanoparticles was conducted by addition of water to a solution of polymer in THF and subsequent slow evaporation of THF (over a time-scale of more than 1 week) to allow the polymer to approach its equilibrium morphology. This process of nanoparticle formation was previously studied by Shimomura and Yabu,[26] and found to be a nucleation and growth process. Under similar conditions, a morphology comprised of parallel lamellae extending to the particle surfaces was initially found. However, if particles were allowed to relax for longer times, this structure changed into concentric lamellae that conformed to the curvature of the particle surfaces.[39] Here, we find that the particle morphology is a concentric layered structure, as shown in Figure 1, consistent with the slow evaporation of THF. Since the PI block is preferentially stained by OsO_4, it appears dark while the PS is bright. The centermost domain was found to be either PI or PS, depending on the overall size of the nanoparticle, as would be expected from previous reports.[18,21] The outer layer of the particles was always PS, suggesting that the water/PS interaction is more favorable than that of water/PI.

TEMT was used to investigate the internal structures of block copolymer nanoparticles in more detail. A tilting series (from $-65°$ to $+65°$ with 1° increment) that were aligned by the fiducial marker method[40] using Au colloids. The mean alignment error, averaged over all fiducial markers used in the alignment, was less than 1 nm (where 1 pixel ~1.0 nm) regardless of the tilt angles. After aligning all the projections, a 3D reconstructed morphology could be generated by the back-projection method[41] to produce a single tomogram. To facilitate viewing of the internal structures, the 3D reconstruction was cut into a hemisphere; as seen in Figure 2 the

morphology consists of onion-like multilayers with some defects. The flattened base of the particle is the result of a slight deformation of particle when it was deposited on the TEM grid. Only the PI component is highlighted, so the PS outer layer is not obvious from these images. A rotating view of the hemisphere is shown in Supporting Information, Movie 1.

2. Morphology Evolution during Solvent Annealing. Starting from the initial state of concentric lamellae, the evolution of the internal structures of block copolymer nanoparticles upon annealing with chloroform vapor was next studied. As shown in Figure 3 and 4, the internal structures undergo dramatic changes with increasing annealing times. From the 2D projections, it can clearly be seen that in a fraction of particles, the concentric lamellar microdomains have broken-up into dots (Figure 3a,b) after 10 min annealing, corresponding to cylindrical or spherical microdomains. An increase in annealing time to 20 min leads to a larger fraction of particles showing break up of lamellae (Figure 3c,d). From Figure 3b,c, it is apparent that this morphological transition occurs more readily for smaller particles, while the larger particles in these images instead show undulation of the concentric rings. Further increases in annealing time, to 30 min (Figure 3e,f),

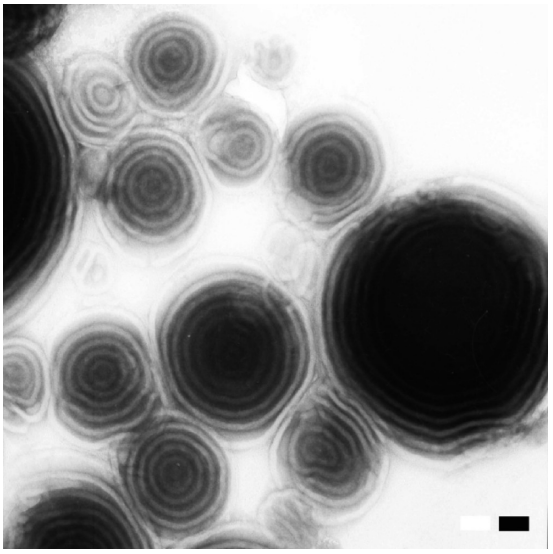

Figure 1. Transmission electron micrograph of block copolymer nanoparticles show concentric alternating layers of PS and PI domains (scale bar: 100 nm). PI domains appear dark due to staining with OsO_4.

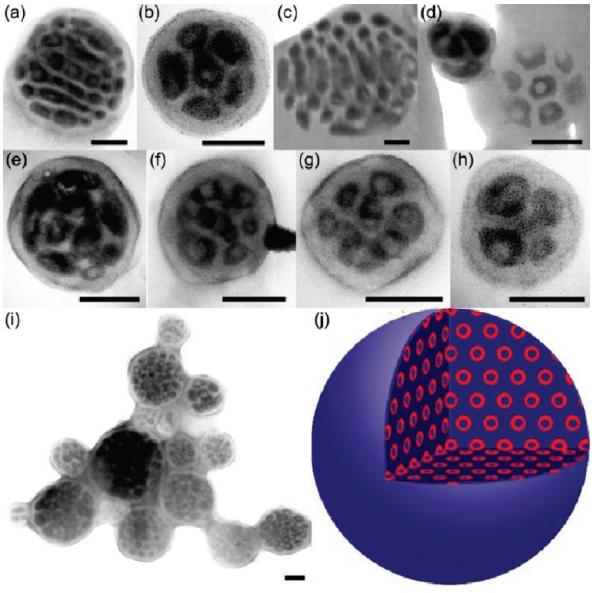

Figure 4. TEM images of morphological transitions of nanoparticles induced by solvent annealing for 12 h (a−d), 26 h (e−h) and 51 h (k) (c and d are nanoparticle cross sectional views), and schematic of dispersed core−shells in particle structure (j) (scale bars: 100 nm).

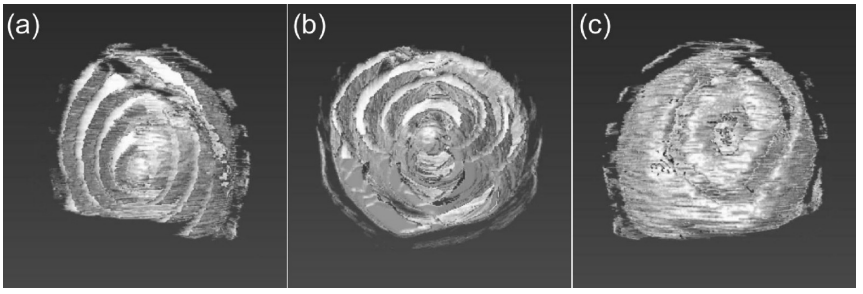

Figure 2. 3D TEMT images of nanoparticles with onion-like microstructures from different viewpoints.

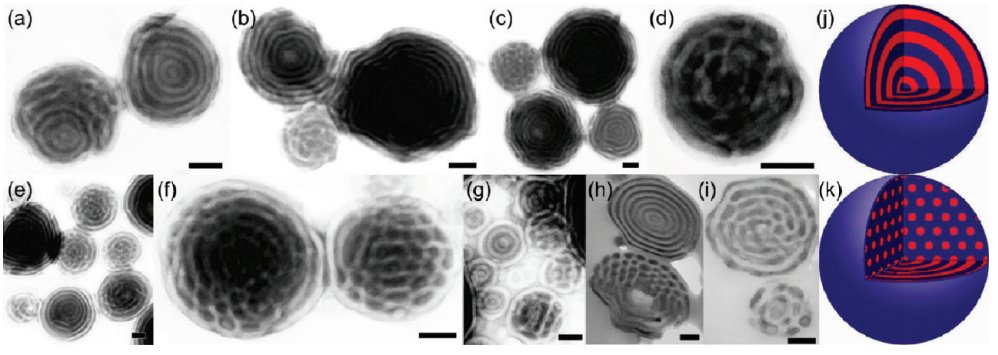

Figure 3. TEM images showing morphological transitions of nanoparticles induced by solvent annealing for 10 min (a, b), 20 min (c, d), 30 min (e, f), 1 h (g−i) (h and i are nanoparticle cross-sectional views) (scale bars: 100 nm), and schematic of onion-like (j) and curved cylindrical structure (k). All samples were stained with OsO_4.

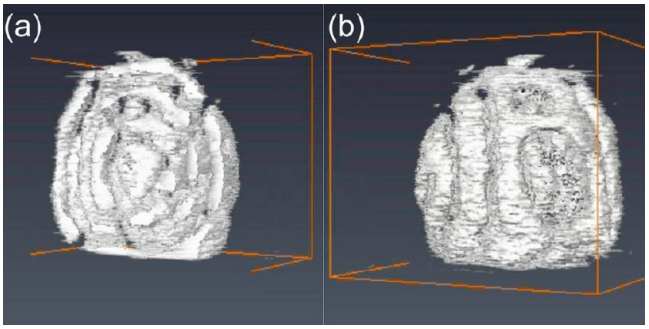

Figure 5. 3D TEMT images of nanoparticles with cylindrical microstructure from different viewpoints.

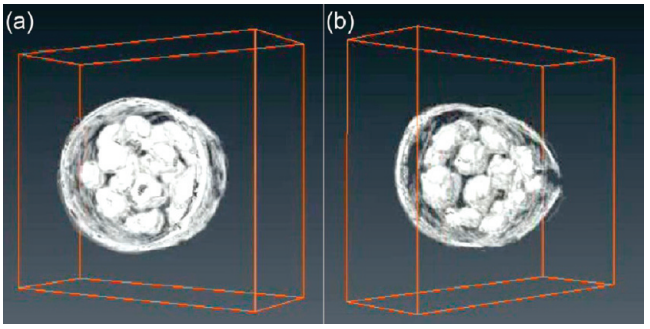

Figure 6. 3D TEMT images of nanoparticles with dispersed core−shell microstructure from different viewpoints.

or 1 h (Figure 3g−i), lead to more prevalent break up of lamellar microdomains, although some fraction of particles retain their concentric structures. Remarkably, the higher magnification images (Figure 3f,i) suggest that some of the dots are not pure PI; but consist of PI shells with PS cores. These PI shell/PS core structures become the dominant morphology after extended annealing times, first exhibiting fairly regular packing of core/shell domains after 12 h of annealing (Figure 4a−d), and subsequently more irregular packing at 26 h (Figure 4e−h) and 51 h (Figure 3i). By this point, almost exclusively core−shell microdomain structures are observed.

To understand the morphological transitions induced by solvent annealing under 3D confinement in more detail, we investigated particles at different transitional stages by TEMT. Particles exhibiting line-and-dot structures in the 2D projections were found to correspond to cylindrical coils wrapping around each other throughout the particles, as shown in Figure 5 and Supporting Information, Movie 2. The lines and dots in Figure 3 correspond to nearly side-on and end-on projections of the cylinders, respectively. The outer layer of PS is again not seen clearly in Figure 5, since the PI domain is stained, although it is apparent from the 2D projections and cross-sectional views in Figure 3. The core−shell particles shown in projection in Figure 4 were confirmed by TEMT to consist of PI-shell/PS-core spherical domains in a PS matrix (Figure 6 and Supporting Information, Movie 3). The highlighted outer skin reflects overstaining of the particle surface by direct exposure to OsO_4 solution vapor; cross-sectional TEM images (Figure 3h and Figure 4d) show no such staining of the surface, indicating that a PS layer is present at the particle surface.

This series of TEMT reconstructions confirmed the transitions from concentric PI lamellae to wrapped PI cylinders and finally to PS/PI core/shell spheres in a PS matrix with increased length of exposure to chloroform vapor. As we discuss in more detail below, we suspect that a slight preference of chloroform to swell PS more than PI shifts the microdomain morphology from a symmetric lamellar to an asymmetric cylindrical structure and even to a spherical structure. The core/shell nature of the ultimate spherical microdomains is an unexpected but reproducible result, which may reflect a kinetically preferred morphology formed upon removal of solvent from disordered solvent-containing nanoparticles.

3. Swelling of Nanoparticles by Chloroform. In our experiments, solvent annealing takes place by vapor-phase exchange of chloroform and water allowing both the aqueous and organic phases to approach saturation with the other solvent. Within the aqueous suspension, chloroform molecules will also diffuse into the polymer nanoparticles, swelling both blocks until the chemical potential of chloroform is equal in each of the microdomains and in the aqueous phase. It is important to note that the chloroform concentration in the aqueous suspension is likely inhomogeneous for short annealing times, which may give rise to the coexistence of particles with different microstructures, as shown in Figure 3. Since larger particles will tend to sediment away from the air/water interface, this could provide at least one mechanism for the size-dependence of the rate of structural transition.

To quantify the degree of swelling of block copolymer nanoparticles in a chloroform-saturated aqueous phase, DLS measurements were performed for different annealing times. The particles confining the BCP have dimensions of several hundred nanometers and their sizes are free to vary with the amount of swelling, thus we refer to the confinement as being induced by "soft" walls. As shown in Figure 7, the diameters of particles increased within the first 2 h of annealing, ultimately reaching an equilibrium degree of swelling corresponding to a 2.5-fold change in volume. Small fluctuations in the measured sizes of the particles are likely due to slight leakage of vapor from the experimental setup and during DLS sample preparation. These swelling data provide useful information to understand the morphological evolution of nanoparticles. Presumably, during the initial stages of swelling, the particles maintain a concentric multilamellar morphology, which upon solvent release leads to the observed undulation of concentric layers. As the particles absorb more solvent and increase further in size, the PI lamellae gradually break up into PI cylinders, likely due to a slightly preferential swelling of PS over PI.

Specifically, the preference of the solvent for one of the blocks can be judged from the difference in polymer and solvent solubility parameters,[42] δ_P and δ_S respectively. Chloroform has a solubility parameter δ of 19.0 $MPa^{1/2}$; literature values of δ for PS range from 17.45 to 19.09 $MPa^{1/2}$ (experimental values at room temperature) from which we determine an average of 18.2 ± 0.6 $MPa^{1/2}$; for PI, δ ranges from 16.2 to 20.46 $MPa^{1/2}$ (experimental values of PI-1,4-*cis* and natural rubber at room temperature) yielding an average of 16.7 ± 0.8 $MPa^{1/2}$. The solubility parameter of chloroform is closer to that of PS than PI, suggesting a slight preference for PS. This affinity should cause PS to swell more than PI and leads to a change in volume ratio, in addition to a decrease of the solvent-mediated effective Flory−Huggins parameter χ_{eff} due to the partition of solvent into both blocks. The increase of ϕ_{PS} due to preferential swelling would clearly provide a driving force to shift to cylindrical PI domains; in addition, since the diblock copolymer is not perfectly symmetric (ϕ_{PS} = 53% and ϕ_{PI} = 47%), decreasing χ_{eff} may also tend to drive the lamellae to cylinder transition. The curvature of the particle surface, coupled with the preferential segregation of PS to the water interface, causes the cylindrical domains to wind around within the particle. With additional swelling, the cylindrical microdomains further

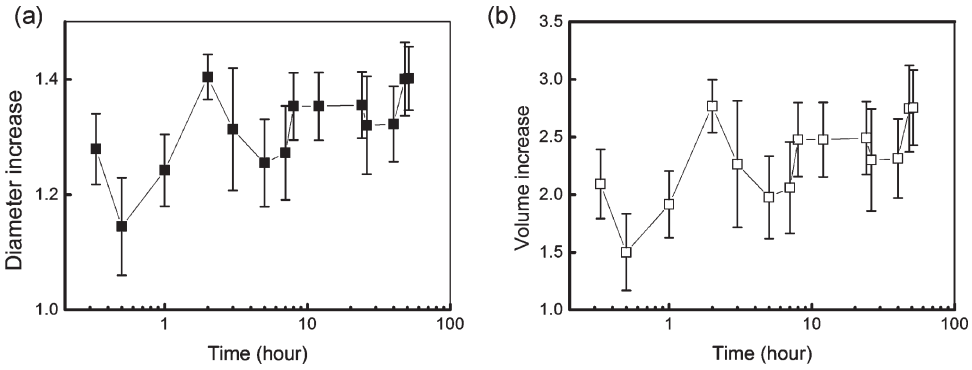

Figure 7. Degree of swelling of nanoparticles during solvent annealing measured by dynamic light scattering: the measured factors by which the average diameter (a) and volume (b) increased are plotted against annealing time.

undergo a transition to spherical domains, though surprisingly with the PI spherical domains containing a core of PS.

Simulations[18−21] on 3D confined BCPs have predicted a rich array of microstructures that are not found in bulk. By varying the surface preference and confinement strength, morphologies including perpendicular lamellar, helical and onion-like morphologies may occur in spherically confined symmetric BCP nanoparticles. With asymmetric BCPs, distorted cylindrical, bicontinuous phases and spherical or peanut-like morphologies can form. Fraaije and co-workers[19] described a morphology diagram for BCP surfactant nanodroplets which included onion-like, bicontinuous, cylindrical, inverted micellar, and phase mixed morphologies with increasing disparities in the volume fractions of the components. The onion-like morphologies observed in our studies agree with the simulations on symmetric BCPs while the morphologies observed in the swollen particles, i.e., cylindrical and micellar, are consistent with the simulations on the asymmetric BCPs.

Diblock copolymers may form different kinds of micelles[43−46] in a selective solvent, where the soluble block stretches and the insoluble block aggregates to minimize the polymer−solvent contact. Spherical micelles[43,45] are common with a long soluble and short insoluble block to minimize the free energy of the system. However, the core−shell morphology is not an equilibrium bulk morphology for diblock copolymers,[47] nor are we aware of previous reports of such structures in solvent-annealed thin films. Typically, when a symmetric BCP thin film is annealed with a neutral solvent the morphology remains lamellar and the film forms terraces due to the incommensurability between the swollen film thickness and the lamellar spacing of the swollen BCP.[35] Selective solvents have been used to shift the volume fractions of the two blocks, leading to cylindrical microdomains oriented parallel or normal to the surface, or dewetting of the swollen film in the case of nonfavorable solvent/substrate interactions.[33,35]

To provide further insight on the factors leading to the unique core−shell morphology, SAXS experiments were performed on bulk samples of the copolymer mixed with similar amounts of chloroform, as in the case of 3D confinement. For a bulk sample of 40 vol % PS-*b*-PI and 60 vol % chloroform, corresponding roughly to the equilibrium 2.5-fold volumetric swelling of nanoparticles, SAXS showed a typical disordered morphology with a correlation hole scattering having a maximum at $\sim$0.3 nm^{-1}. If the BCP is in the disordered state after attaining the equilibrium degree of swelling, this suggests that the core−shell morphology is likely formed during the removal of the solvent from the particle and is kinetically trapped. When chloroform is removed from the swollen particle, ordering propagates from the particle surface to the center, due to the slight selectivity of chloroform for the PS block. A layer of PS is formed on the surface of the particle in order to reduce the interfacial energy and, due to the connectivity of the blocks, a layer of PI forms immediately underneath this. Since the concentration of solvent is lowest on the surface, this ordering can occur on the surface while the interior of the particle is still disordered where solvent is mediating segmental interactions. As solvent evaporation continues, the microphase separation continues driving the formation the of core−shell morphology.This microphase separation has occurred, of course, under the constraints of an ever-decreasing volume which introduces commensurability issues the length scale and curvature of the confining volume and the equilibrium strucute of the block copolymer. In addition, the microphase separation will be arrested when the T_g of the PS microdomains is at room temperature. All of these factors can and will give rise to morphologies that are very far-removed from their equilibrium morphology.

Conclusions

Nanoparticles with concentric onion-like morphology were prepared from a lamellae-forming PS-*b*-PI diblock copolymer via controlled precipitation from a good/poor solvent mixture. Chloroform was introduced to an aqueous suspension of the particles through the vapor phase, leading to morphological transitions as characterized by 3-D reconstructions obtained by TEMT. Presumably due to a slight selectivity of chloroform for PS, the concentric lamellae first broke up to yield PI cylinders wrapped around within the nanoparticles, and subsequently into spherical domains. These morphologies are in keeping with recent simulation results, with the exception of the unpredicted core−shell nature of the spherical domains, which we suggest form upon removal of solvent from disordered BCP nanoparticles swelled to equilibrium with solvent. The results shown here demonstrate a useful new methodology for tuning structure in 3D confined BCPs and underscore the importance of solvent quality in generating unique morphologies in such systems. The resulted well-defined morphologies can be produced that have potential applications in drug delivery, photonics, aerosols, templates for catalysts, and food industry. Additionally, future efforts to tune the equilibrium degree of swelling through solvent activity, as well as to use more highly selective solvents, are anticipated to provide powerful routes to control the morphology of 3D confined block copolymers.

Acknowledgment. We acknowledge the support of the Word Premier International Research Center-Advanced Institute for Materials Research (WPI-AIMR) in Tohoku University. H.J. is grateful for support from the Ministry of Education, Science, Sports and Culture through Grant-in-Aid No. 21015017,

No. 21106512 and No. 21241030. This work was funded by the US National Science Foundation through the MRSEC at the University of Massachusetts Amherst (DMR-0820506) and Grant CBET-0931616 and by the Office of Basic Energy Science of the US Department of Energy.

Supporting Information Available: 3D TEMT movies (.avi) showing onion-like (1), cylindrical (2), and dispersed core−shell (3) structures. This material is available free of charge via the Internet at http://pubs.acs.org.

References and Notes

(1) Bates, F. S.; Fredrickson, G. H. *Annu. Rev. Phys. Chem.* **1990**, *41*, 525–557.
(2) Russell, T. P. *Curr. Opin. Colloid Interface Sci.* **1996**, *1* (1), 107–115.
(3) Matsen, M. W. *J. Chem. Phys.* **1997**, *106*, 7781–7791.
(4) Fasolka, M. J.; Mayes, A. M. *Annu. Rev. Mater. Res.* **2001**, *31*, 323–355.
(5) Cheng, J. Y.; Ross, C. A.; Thomas, E. L.; Smith, H. I.; Vancso, G. J. *Appl. Phys. Lett.* **2002**, *81*, 3657–3659.
(6) Segalman, R. A. *Mater. Sci. Eng. R-Rep.* **2005**, *48* (6), 191–226.
(7) Sevink, G. J. A.; Zvelindovsky, A. V.; Fraaije, J.; Huinink, H. P. *J. Chem. Phys.* **2001**, *115*, 8226–8230.
(8) Yu, B.; Sun, P. C.; Chen, T. C.; Jin, Q. H.; Ding, D. T.; Li, B. H.; Shi, A. C. *Phys. Rev. Lett.* **2006**, *96* (13).
(9) Chen, P.; He, X. H.; Liang, H. J. *J. Chem. Phys.* **2006**, *124* (10).
(10) Feng, J.; Ruckenstein, E. *Macromolecules* **2006**, *39*, 4899–4906.
(11) Li, W. H.; Wickham, R. A. *Macromolecules* **2006**, *39*, 8492–8498.
(12) Xiang, H. Q.; Shin, K.; Kim, T.; Moon, S. I.; McCarthy, T. J.; Russell, T. P. *Macromolecules* **2004**, *37*, 5660–5664.
(13) Wu, Y. Y.; Cheng, G. S.; Katsov, K.; Sides, S. W.; Wang, J. F.; Tang, J.; Fredrickson, G. H.; Moskovits, M.; Stucky, G. D. *Nat. Mater.* **2004**, *3* (11), 816–822.
(14) Sun, Y. M.; Steinhart, M.; Zschech, D.; Adhikari, R.; Michler, G. H.; Gosele, U. *Macromol. Rapid Commun.* **2005**, *26*, 369–375.
(15) Xiang, H.; Shin, K.; Kim, T.; Moon, S. I.; McCarthy, T. J.; Russell, T. P. *Macromolecules* **2005**, *38*, 1055–1056.
(16) Ma, M. L.; Krikorian, V.; Yu, J. H.; Thomas, E. L.; Rutledge, G. C. *Nano Lett.* **2006**, *6*, 2969–2972.
(17) Thomas, E. L.; Reffner, J. R.; Bellare, J. *J. Phys.* **1990**, *51*, C7363–C7374.
(18) He, X. H.; Song, M.; Liang, H. J.; Pan, C. Y. *J. Chem. Phys.* **2001**, *114*, 10510–10513.
(19) Fraaije, J.; Sevink, G. J. A. *Macromolecules* **2003**, *36*, 7891–7893.
(20) Chen, P.; Liang, H. J.; Shi, A. C. *Macromolecules* **2008**, *41*, 8938–8943.
(21) Yu, B.; Li, B. H.; Jin, Q. H.; Ding, D.; Shi, A. C. *Macromolecules* **2007**, *40*, 9133–9142.
(22) Okubo, M.; Saito, N.; Takekoh, R.; Kobayashi, H. *Polymer* **2005**, *46*, 1151–1156.
(23) Saito, N.; Takekoh, R.; Nakatsuru, R.; Okubo, M. *Langmuir* **2007**, *23*, 5978–5983.
(24) Jeon, S. J.; Yi, G. R.; Koo, C. M.; Yang, S. M. *Macromolecules* **2007**, *40*, 8430–8439.
(25) Jeon, S. J.; Yi, G. R.; Yang, S. M. *Adv. Mater.* **2008**, *20*, 4103–4108.
(26) Yabu, H.; Higuchi, T.; Ijiro, K.; Shimomura, M. *Chaos* **2005**, *15* (4).
(27) Higuchi, T.; Tajima, A.; Motoyoshi, K.; Yabu, H.; Shimomura, M. *Angew. Chem., Int. Ed.* **2008**, *47*, 8044–8046.
(28) Arsenault, A. C.; Rider, D. A.; Tetreault, N.; Chen, J. I. L.; Coombs, N.; Ozin, G. A.; Manners, I. *J. Am. Chem. Soc.* **2005**, *127*, 9954–9955.
(29) Rider, D. A.; Chen, J. I. L.; Eloi, J. C.; Arsenault, A. C.; Russell, T. P.; Ozin, G. A.; Manners, I. *Macromolecules* **2008**, *41*, 2250–2259.
(30) Mansky, P.; Liu, Y.; Huang, E.; Russell, T. P.; Hawker, C. J. *Science* **1997**, *275* (5305), 1458–1460.
(31) Thurn-Albrecht, T.; DeRouchey, J.; Russell, T. P.; Jaeger, H. M. *Macromolecules* **2000**, *33*, 3250–3253.
(32) Niu, S. J.; Saraf, R. F. *Macromolecules* **2003**, *36*, 2428–2440.
(33) Xuan, Y.; Peng, J.; Cui, L.; Wang, H. F.; Li, B. Y.; Han, Y. C. *Macromolecules* **2004**, *37*, 7301–7307.
(34) Kim, S. H.; Misner, M. J.; Xu, T.; Kimura, M.; Russell, T. P. *Adv. Mater.* **2004**, *16*, 226–231.
(35) Peng, J.; Kim, D. H.; Knoll, W.; Xuan, Y.; Li, B. Y.; Han, Y. C. *J. Chem. Phys.* **2006**, *125* (6).
(36) Jinnai, H.; Nishikawa, Y.; Ikehara, T.; Nishi, T. *Adv. Polym. Sci.* **2004**, *170*, 115–167.
(37) Jinnai, H.; Spontak, R. J.; Nishi, T. *Macromolecules* **2010**, *43*, 1675–1688.
(38) Nishioka, H.; Niihara, K. I.; Kaneko, T.; Yamanaka, J.; Inoue, T.; Nishi, T.; Jinnai, H. *Compos. Interfaces* **2006**, *13*, 589–603.
(39) Yabu, H.; Higuchi, T. Personal communication about morphological manipulations of block copolymer nanoparticles formed via controlled precipitation from a good/poor solvent mixture, **2008**.
(40) Luther, P. K.; Lawrence, M. C.; Crowther, R. A. *Ultramicroscopy* **1988**, *24* (1), 7–18.
(41) Frank, J., *Electron Tomography: Three-Dimensional Imaging with the Transmission Electron Microscope*. Springer: New York, 1992.
(42) Brandrup, J.; E. H. I., *Polymer Handbook*, 3rd ed.; John Wiley and Sons: New York, 1999.
(43) Ding, J. F.; Liu, G. J. *J. Phys. Chem. B* **1998**, *102*, 6107–6113.
(44) Ding, J. F.; Liu, G. J. *Macromolecules* **1997**, *30*, 655–657.
(45) Zhang, L. F.; Eisenberg, A. *Science* **1995**, *268* (5218), 1728–1731.
(46) Ding, J. F.; Liu, G. J.; Yang, M. L. *Polymer* **1997**, *38*, 5497–5501.
(47) Matsen, M. W.; Bates, F. S. *Macromolecules* **1996**, *29*, 7641–7644.